ADVANCED SUSTAINABLE SYSTEMS
www.advsustainsys.com

High Performance Triboelectric Nanogenerators from Compostable Cellulose-Biodegradable Poly(Butylene Succinate) Composites

Linards Lapčinskis, Līva Ģērmane, Oskars Platnieks, Artis Krikovs, Sergejs Gaidukovs, Kaspars Pudzs, Artis Linarts, Peter C. Sherrell, and Andris Šutka**

Triboelectric nanogenerator (TENG) devices are exemplar systems for mechanical-to-electrical energy conversion due to their simplicity and promising performance. However, little attention has been paid to recycling or reusing TENG devices. Indeed, most TENG devices are based on non-biodegradable polymers, and thus end up in a landfill. Developing biodegradable triboelectric materials is crucial to mitigate negative environmental impacts from their growing use, however, it is challenging to identify such a materials that generate an applicable charge. Herein, such a biodegradable polymer triboelectric pair is demonstrated, by combining poly(butylene succinate) (PBS) films with microcrystalline cellulose (MCC) filler. A power density of 143 mW m^{-2} and a charge density of 1.36 nC cm^{-2} is measured when contacting pristine PBS with 70 wt% MCC/PBS composite film, which is comparable to polydimethylsiloxane-based TENGs under identical testing conditions. These devices are shown to degrade via composting at 58 °C over 70 days, enabling long-term (>10 000 cycle) performance and degradation upon disposal. It is suggested that this approach can be extended to control triboelectric properties for other biodegradable polymers. The technology and concepts developed herein directly address the United Nations Sustainable Development Goals for Responsible Consumption & Production and Affordable and Clean Energy.

1. Introduction

Triboelectric nanogenerators (TENGs) are promising flexible mechanical-to-electrical energy harvesters that have attracted significant attention over the past decade.[1] TENG devices can be applied for powering autonomous microdevices,[2] powering the growing Internet of Things (IoT) sector,[3] robotics,[4] bionics,[5] or even to drive water-splitting electrolyzers.[6,7]

In a typical TENG device, conductive electrodes are covered by a pair of materials (typically polymers) that gain an equal but opposite surface charge when brought into contact and separated from each other. The formation of triboelectric surface charges results in charge induction on the conductive electrodes. With the variable electric potential of this charge induction during motion being balanced by current flow in the external circuit. Using this simple contact-separation process, TENGs have shown

L. Lapčinskis, A. Šutka
Institute of Materials and Surface Engineering
Faculty of Materials Science and Applied Chemistry
Riga Technical University
P. Valdena 3/7, Riga LV-1048, Latvia
E-mail: andris.sutka@rtu.lv

L. Lapčinskis, L. Ģērmane, A. Linarts
Institute of Technical Physics
Faculty of Materials Science and Applied Chemistry
Riga Technical University
P. Valdena 3/7, Riga LV-1048, Latvia

O. Platnieks, A. Krikovs, S. Gaidukovs
Institute of Polymer Materials
Faculty of Materials Science and Applied Chemistry
Riga Technical University
P. Valdena 3/7, Riga LV-1048, Latvia

K. Pudzs
Institute of Solid State Physics
University of Latvia
Kengaraga str. 8, Riga LV-1063, Latvia

P. C. Sherrell
School of Chemical and Biomedical Engineering
Faculty of Engineering and Information Technology
The University of Melbourne
Parkville 3010, Australia
E-mail: peter.sherrell@rmit.edu.au

P. C. Sherrell
School of Science
STEM College
RMIT University
Melbourne 3001, Australia

The ORCID identification number(s) for the author(s) of this article can be found under https://doi.org/10.1002/adsu.202300280

DOI: 10.1002/adsu.202300280

to generate enough power that could potentially power a smartwatch.[8,9]

Currently, materials used in TENG devices are based on synthetic and non-biodegradable polymers, such as polydimethylsiloxane (PDMS),[10] polytetrafluoroethylene (PTFE),[11] and polyvinylidene fluoride (PVDF).[12] These materials have been widely studied and are known for their high triboelectric performance, durability, and stability.

However, the use of these materials in TENGs leads to significant plastic waste at their end-of-life cycle, and thus are in opposition to the United Nations Sustainable Development Goals of Responsible Consumption and Production. Further, one of the primary mechanisms for charge generation in polymer TENGs is mass transfer, whereby charge oligomer fragments are generated by bond scission at the contact-separation interface.[13–15] While these charged oligomers, in combination with other charge transfer processes,[16] lead to the exception surface charge densities from polymer TENGs, they may contribute to the emergent microplastic pollution emergency,[17] particularly for TENGs designed to operate in water.[5–7] Interestingly, the electrostatic field generated by TENGs has also been shown to be efficient in removing these microplastics from water, potentially tied to that same material transfer mechanism.[18] Thus, making a TENG from biodegradable and/or recyclable polymers is highly desirable to decrease environmental impact. Several types of biodegradable polymers have been explored for use in TENGs including polylactic acid (PLA),[19] poly[(R)−3-hydroxybutyric acid] (PHB),[20] chitosan,[21] cellulose derivatives,[22–27] silk,[28] hyaluronic acid,[29] starch,[30] polycaprolactone,[30] wood,[31,32] and others.[33] For example, Hao et al. demonstrated a biodegradable TENG device based on contact layers of wood and PTFE which generated maximum power output of 158.2 mW m^{-2}.[32] Similarly, Zhang et al. describes a TENG device that employs surface modified cellulose nanofibrils (CNF) contacted against fluorinated ethylene propylene (FEP) polymer to reach power output of 430 mW m^{-2}.[23] Generally, many TENG devices termed biodegradable based on cellulose derivatives have been reported to reach power density close to 1 W m^{-2},[22] however in these cases the biodegradable polymer is contacted against a non-biodegradable and environmentally hazardous fluoropolymer (either PTFE or FEP). TENG devices made wholly from biodegradable polymer contact pairs such as wood-based TENG have been shown to reach lower power densities, i.e., close to 135 mW m^{-2}.[31]

While promising forays into the TENG field, these materials are unoptimized requiring significant research to enhance their performance and stability in TENGs. To observe the triboelectric output, two materials with distinctive surface properties must be combined in TENG devices.[30] This increases the complexity of design significantly. Further, biodegradable polymers typically lie close together on the triboelectric series, this means that contact between dissimilar biodegradable polmyers will only generate moderate surface charge.[34] Recently, we have established benchmarks in engineering polymer surfaces to enhance triboelectric surface charge via additives,[35] macromolecular ordering[36] and roughness,[37] which can be used to dramatically enhance the charge output from a given polymer pair using simple approaches. We propose these techniques can be applied to biodegradable same-material biodegradable polymers to make sustainable TENG devices with competitive energy outputs.

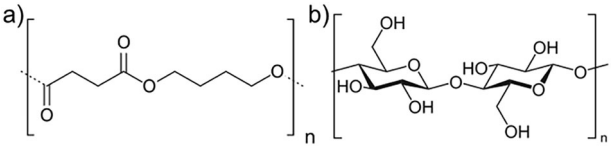

Scheme 1. Chemical structure of a) PBS and b) Cellulose.

Here, we study the triboelectric charge generated between, biodegradable polybutylene succinate (PBS) films, where one of the PBS layers is modified by a biodegradable microcrystalline cellulose (MCC) filler. By tuning the amount of MCC in a PBS film the surface charge is enhanced by 25x compared to pristine PBS. The MCC/PBS composites are demonstrated to degrade to less than 20% of their initial mass under composting at 58 °C within 70 days. This thermally activated composting degradation allows the TENG devices to function for 10 000 cycles, yet degrade once disposed of. The measured surface charge is shown to be approximately proportional to the difference in elastic modulus of each contacting pair. The power density of TENG devices based on pristine PBS and PBS/MCC composite reaches 143 mW m^{-2}. Furthermore, this work reports TENG output comparable to state-of-the-art TENGs based on biodegradable materials by using same-material contact electrification, enabling the expansion and use of MCC in other biodegradable polymers to enhance charging.[31] This study demonstrates a proof of concept approach to engineer biodegradable TENGs, simultaneously addressing the United Nations Sustainable Development Goals of Affordable and Clean Energy and Responsible Consumption and Production.

2. Experimental Section

2.1. Materials

BioPBS FZ71PB is a bio-based and biodegradable PBS resin, produced by PTT MCC Biochem Company Ltd., suitable for thermoplastic extrusion and injection molding processing and industrial applications. PBS has a density of 1.26 g cm^{-1},[3] a melt flow index of 22 g per 10 min [190 °C, 2.16 kg], and a melting point of 115 °C. Nisshinbo Chemical Inc. supplied Carbodilite® HMV-15CA. According to manufacturer information, it contains a carbodiimide (CDI) group, which works as a chain extender and hydrolysis stabilizer. STRUKTOL® TPW 709 (abbreviated as STR) was purchased from Struktol LLC. and is a processing additive for producing extruded polymer/wood composites. The recommended dosage level is 1–4 wt.% depending on the percent and species of wood in the formulations. Cold pressed extra virgin rapeseed oil produced locally (Iecavnieks, Latvia) was used for synthesis. MCC was produced from bleached softwood kraft pulp (Metsä Botnia AB, Finland). The chemical structures of employed materials are shown in **Scheme 1**.

2.2. MCC Preparation and Rapeseed Oil Acrylation

MCC was obtained according to the procedure reported previously by the authors.[38] In compliance with this method, the

Table 1. Samples compositions.

Sample	PBS [wt.%]	MCC [wt.%]	STR [wt.%]	ARO [wt.%]
PBS	100	–	–	–
10 wt.% MCC/PBS	86.54	9.62	0.96	2.88
30 wt.% MCC/PBS	67.31	28.85	0.96	2.88
50 wt.% MCC/PBS	48.08	48.08	0.96	2.88
70 wt.% MCC/PBS	28.85	67.31	0.96	2.88

pulp was impregnated with a thermocatalytic degradation catalyst – weak hydrochloric acid solution (0.05%) and ground in a ball mill "U.S. Stoneware JAR MILL 755RMV1" (USA) with variable speed. According to SEM analysis, the average size of MCC particles is 10–40 μm.[38]

Rapeseed oil (RO) was used as received. Synthesis was performed with the previously reported method.[39] In a two-neck round-bottom flask, RO (50.0 g) was mixed with acrylic acid (AA) (33.2 g), and catalyst BF_3OEt_2 (5.7 mL) was gradually added dropwise. The mixture was continuously stirred, allowed to react for 5 h at 80 °C, and then left at room temperature overnight. The organic phase was then dissolved using n-hexane, and the unreacted AA and catalyst were separated using a $NaHCO_3$ solution. After that, the product was filtered and dried. Finally, N-hexane was removed with a rotary evaporator, resulting in a yellowish liquid called acrylated rapeseed oil (ARO).

2.3. Preparation of Composites

PBS granules and MCC powder were dried in a vacuum furnace (J.P. Selecta) at 60 °C (5–20 mbar) for 8 h before further processing. Compounding of the PBS/MCC composites was carried out on a thermoplastic mixer Brabender® Mixer 50EHT (Germany). Premixed compositions were used and the composite abbreviations for each composition are shown in **Table 1**. Abbreviations reflect the weight ratio between cellulose and PBS. The processing conditions were adjusted to 70 rpm for twin screws, heating in all zones was 140 °C with melt blending time fixed to 7 min.

Composite films were prepared with compression molding technique using Carver CH 4386. The temperature for hot plates was set at 140 °C, the samples were preheated for 2 min, compressed for 3 min (3 MT pressure), and cooled for 3 min between steel plates (30 kg of thermal conductive mass).

2.4. Tensile Testing Methods

Tensile characteristics were measured by adapting ISO 527 using the Tinius Olsen model 25ST (Horsham, PA, USA) equipped with a 5 kN load cell. Five parallel measurements were performed with a 1 mm min^{-1} testing crosshead speed at 20 °C and 50% relative humidity. Tests were conducted on composite film strips with dimensions of length = 50.0 mm, width = 10.0 mm, and thickness = 0.1 mm.

2.5. Differential Scanning Calorimetry

A differential scanning calorimeter (DSC) (Mettler DSC-1) was used to evaluate the melting processes. Specimens with a weight of ≈10 mg were used and sealed in an aluminium pan. The samples were heated from 25 to 150 °C at a rate of 10°C min^{-1}. The crystallinity of the PBS and the composites was calculated from the first heating thermogram data according to the equation:

$$\chi = \frac{\Delta H_c}{\Delta H_m^o \left(1 - W_F\right)} \times 100\% \quad (1)$$

where ΔH_c is the enthalpy of the specimen from the melting peak, ΔH_m^o is the theoretical melting enthalpy of 100% crystalline polymer (110.5 J g^{-1} for PBS)[40] and W_F is the weight content of fillers.

2.6. Electric Measurements

Unless specifically mentioned, the triboelectric measurements were made under controlled conditions – a separation distance of 5 mm, a pressing force of 10 N, and a contact-separation frequency of 1 Hz. To ensure repeatability, contact-separation was carried out using an Instron E1000 material testing machine. The generated current signals were measured using Keithley 6514 electrometer connected to a Picoscope 5444B PC oscilloscope system. The charge generated by individual films was determined after contact-separation with ITO which was connected to an electrometer and the current was measured against the ground.

The pristine PBS and PBS composite films were next used to prepare TENG devices. In this case, both electrodes were connected to an electrometer. Surface charges, Q (nC), were calculated from the measured current peaks using the equation $Q = \int i dt$, where i is the instantaneous current (nA) and dt is the differential of time (s). Integration was done for the high, narrow peaks which correspond to the separation stage.

Instantaneous power was calculated using $P = V^2 R^{-1}$ from the data obtained in voltage measurements at the corresponding load resistance R. Next, the instantaneous power was plotted as a function of time. Integration of peak area allowed to calculate the energy generated during separation. The peak duration was also determined from the plot and used to calculate the average power during the separation step using $P = E \times \Delta t^{-1}$. Energy density and power density were calculated by dividing energy and power by the sample contact area.

The AC signal from TENG was rectified using a full bridge rectifier and then directed to a capacitor. The voltage across capacitors was measured using Keithley 6514 electrometer connected to a Picoscope 5444B PC oscilloscope. Energy E (nJ) stored in the capacitor was calculated using equation $E = 0.5CV$,[2] where C is the capacitance of the capacitor (nF) and V is the voltage across the capacitor (V).

For high-speed contact separation, a pneumatic device from custom made PLC controlled (Mitsubishi AL2-24MR-D) pneumatic system, utilizing a low friction smooth cylinder actuator (SMC MQML10) capable of producing 16 N contacting force and high translation speed (1000 mm s^{-1}) was used. Additionally, a Faraday cage was placed around the triboelectric testing area to eliminate parasitic signals. All samples were measured in constant ambient relative humidity (35%).

Kelvin probe measurements were performed using the Scanning Kelvin Probe system SKP5050. The surface potential of the

sample was scanned by oscillating a 2 mm radius tip in a 3-by-3 point area (total 9 points) to obtain surface potential maps. The distance between two scanned points was ≈1 mm.

2.7. Biodegradation Testing

A laboratory balance test was carried out to characterize biodegradation in composting conditions. Compost soil (swamp peat) with a pH of 6.5 was acquired from a local distributor, Biolan Baltic (Pärnu, Estonia). The aerobic conditions were maintained at 58 °C and 55% soil humidity. A 58 °C temperature was selected for comparison to tests carried out according to ISO 14855, ISO 20200, and ASTM D 6400 standards for bacterial-based biodegradation. Films with a thickness of 100 μm were cut into squares (25 mm × 25 mm), which were encased between sieves and deposited in the soil at a depth of 1.5 cm using closed plastic containers. For each sample, six parallel specimens were put together. Three samples were recovered every 10 days, dried in a vacuum oven at 60 °C for 4 h, weighed, photographed, and inserted back into the soil. An average weight loss between the three samples was used. Tests were carried out till it was impossible to separate films from the soil (up to 80 days).

2.8. Morphology Analysis

The composites' microstructures were investigated utilizing a scanning electron microscope (SEM) model Phenom Desktop SEM, operating at an acceleration voltage of 15 kV. The analysis involved employing the liquid nitrogen-fractured surfaces of the composites as the specimen for measurements.

2.9. FTIR Analysis

The investigation of PBS, MCC, and composites involved the application of Fourier transform infrared spectroscopy (FTIR) in attenuated total reflectance mode. The analysis was conducted within the spectral range of 600–4000 cm^{-1}, employing a Nicolet 6700 instrument (ThermoScientific) with a resolution set at 4 cm^{-1}. To ensure accuracy, sixteen measurements were performed, resulting in a measurement error of 1%, and the displayed spectrum represents the average of these measurements.

3. Results and Discussion

To develop and characterise a biodegradable TENG, the triboelectric properties of PBS with varied concentrations [between 0% and 70% by mass] of microcrystalline cellulose (MCC) filler were studied. The filler was added to change the deformative properties of the PBS during contact-separation, both bulk properties but also to induce heterogenous regions of stress concentration.[36] Surface contact charge formation is enhanced when polymers with distinct deformative (mechanical) properties are contact-separated.[35,37,41] The changes in surface morphology of composites with increasing MCC content are minor (Figure S1, Supporting Information). At mass loadings below 70 wt.%, a small increase in surface porosity and irregular pores are observed, however, at 70 wt.% MCC composite the maximum filler content is reached and MCC filler particles are observed sticking out of composite surface. A similar conclusion can be made from AFM studies, for the pristine PBS (0 wt.% MCC) the mean surface roughness (Sa) was 51.4 ± 10.1 nm (Figure S2, Supporting Information). The addition of MCC in the composite correlates to an increase in the roughness, it steadily increased to 175.6 ± 24.5 nm for 70 wt.% MCC composite due to presence of pores and particles on surface. While changes in surface roughness may indeed contribute to increased surface charge density,[37,41,42] we are confident that the main contributing factor in this case is the difference in mechanical properties due to filler addition.

To further understand the effect of fillers on the morphological and mechanical properties of the biodegradable PBS composites, FTIR, SEM and mechanical testing were performed, with these properties later correlated with triboelectric surface charge.

3.1. FTIR Analysis

To investigate the chemical structure of obtained PBS/MCC composites, FTIR measurements were conducted (**Figure 1**a). The decrease in the relative intensity of the PBS carbonyl peak at 1712 cm^{-1} with increasing MCC content (Figure 1b), along with the enhancement of the shoulder peaks at 1720 and 1730 cm^{-1} demonstrate a clear interaction between the MCC and the PBS matrix.[43] The carbonyl peak is prone to robust intermolecular interactions with cellulose molecules, such as hydrogen bonding with cellulose hydroxyl groups. Similarly, analogous observations can be made for the peak at 1151 cm^{-1}, commonly attributed to PBS C—O or C—O—C asymmetric stretching vibrations.[43] For further comprehensive insights into the breakdown of PBS and cellulose spectra, a detailed analysis can be explored in the literature.[44]

3.2. Morphology

To understand the interaction between MCC and PBS within the samples, liquid nitrogen fracturing of the composite films was performed. The resultant surfaces were imaged via SEM (**Figure 2**) which illustrate that PBS/MCC composites exhibit pronounced morphology variations at different MCC loadings. The composite containing 10 wt.% MCC displays a uniform dispersion of MCC particles with minimal apparent agglomeration. The presence of minute voids within the structure suggests particle pull-outs during fracture events. Similarly, the 30 wt.% MCC composite reveals relatively well-dispersed particles. Upon reaching a loading of 50 wt.% MCC, some degree of agglomeration is evident. Notably, the MCC particle size distribution ranges from 5 to 30 μm. However, particles on the crosscut surface affected by the fracture route show some separation and gaps between MCC particles and the PBS matrix, an expected consequence of crack propagation during fracture in the interface when ARO compatibilizer content becomes insufficient due to the introduction of high-loading cellulose filler loadings in the polymer. Despite the high loadings, the distribution of MCC particles within the PBS

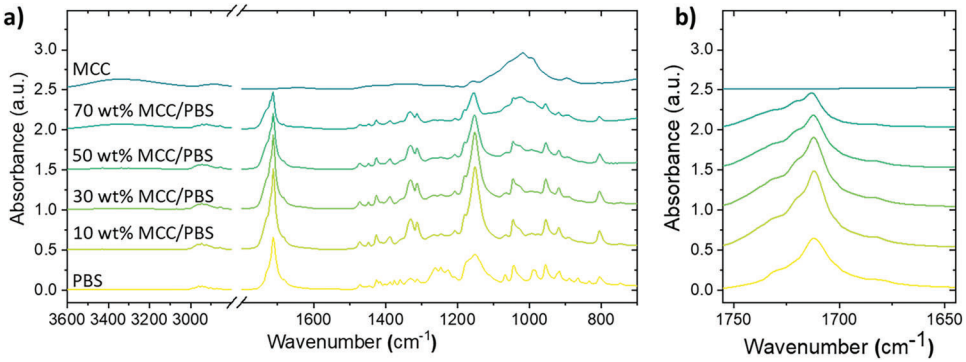

Figure 1. a) Full FTIR spectra and b) spectra of the peak at 1712 cm^{-1} for PBS, MCC, and composites.

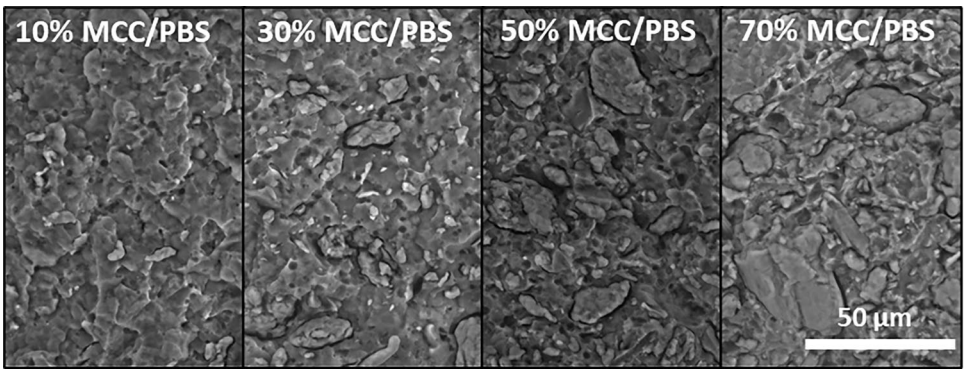

Figure 2. SEM micrographs of the fracture surface of PBS/MCC composites.

matrix remains relatively uniform up to 70% MCC content, with some limited agglomerate formation. Additionally, the SEM images uncovers a complex route of crack propagation and a highly irregular fracture surface. Notably, no visible defects were detected in the MCC particles, suggesting that fracture formation is primarily associated with failure at either the PBS matrix or the PBS/MCC interface.

3.3. Mechanical Properties

The elastic modulus (E), tensile strength (σ), and elongation at break (ϵ) for the melt blended PBS and PBS/MCC composites are shown in **Figure 3**. The addition of stiff cellulose particles (1–2 GPa)[45] significantly increases the elastic modulus values from 277 MPa for pure PBS (0% MCC) up to 1310 MPa for a PBS/MCC composite (70 wt.% MCC) (Figure 3a). The increase in elastic modulus scales almost linearly with the higher MCC loading, modulus grows by ≈14 MPa per added wt.% of MCC. Tensile strength shows a similarly linear drop that correlates with higher MCC loadings, from 29 MPa (0% MCC) to 7 MPa (70% MCC) (Figure 3b). In this case, tensile strength decreases by 0.3 MPa per added wt.% of MCC. These linear trends clearly show the PBS/MCC composites are following the rule of mixtures for mechanical properties, and thus there is strong interfacial binding between PBS chains and MCC particles due to incorporation of ARO modifier that leading to effective load transfer.[46]

The elongation at break, denoted by the strain, shows a nonlinear relationship with MCC content. At MCC wt.% > 50, a sharp drop in strain values is observed, which is an effect of depressed polymer plastic deformation due to hindered chain mobility and internal defects (Figure 3c).[47] These trends show that in terms of mechanical properties, 0% and 70% MCC content PBS have vastly different deformative structural properties and can be expected to generate significant surface charge as a contact-separation pair. The authors note that TENGs operating in contact-separation mode are in the compressive regime of mechanical properties, and thus the increased brittleness of high MCC content PBS is not expected to lead to further device failure during use.

3.4. Crystallinity

The effect of MCC filler loading on the melting temperature (T_m) and crystallinity (χ) was investigated through DSC analysis. The DSC first heating scan is shown in Figure S3 (Supporting Information), and the obtained values are summarized in **Table 2**. The DSC curve shows a small exothermic peak at ≈90 °C; this peak has been attributed in the literature to the recrystallization of imperfectly formed crystalline regions.[48] Following the small exothermic peak, there is a large endothermic peak representing the melting of the PBS crystalline phase. In the case of PBS, it has been reported that the melting peak consists of two separate peaks, which represent the melting of imperfect crystalline regions, followed by the main melting peak, which represents the melting of the crystalline PBS structure.[49] The MCC loading significantly affects the crystallinity of PBS. At lower loadings, crys-

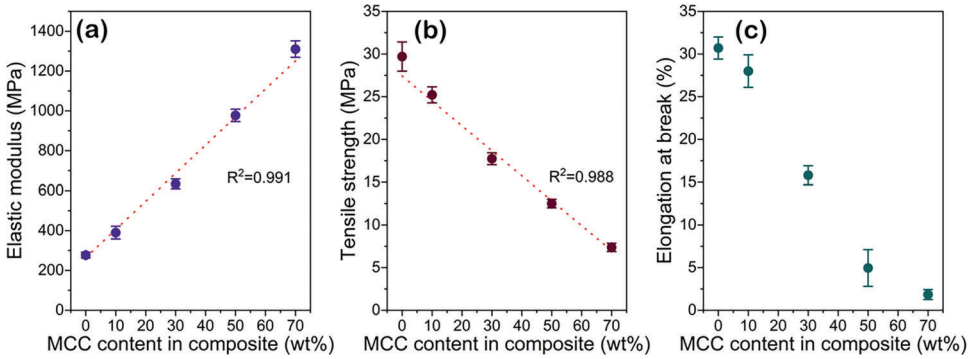

Figure 3. Tensile properties: a) elastic modulus, b) tensile strength, and c) elongation at break for PBS and PBS/MCC composites.

Table 2. Calorimetric properties of PBS and PBS/MCC composites.

Sample	ΔH_m [J/g]	χ [%]	T_m [°C]
PBS	79.8	72.2	116.3
10 wt.% MCC/PBS	64.0	66.9	116.1
30 wt.% MCC/PBS	53.0	71.1	116.7
50 wt.% MCC/PBS	39.1	73.5	115.3
70 wt.% MCC/PBS	25.0	78.3	114.9

tallinity is slightly reduced, but the melting temperature remains high, close to the pure PBS value of 116.3 °C. Starting from loadings where the PBS and MCC ratio is 1 to 1, a notable shift in peak shape can be observed as it shifts to lower temperatures. This indicates that MCC disrupts the formation of the crystalline phase, yielding more imperfect lamella structures. But at the same time, crystallinity values increase, which indicates that MCC promotes the crystallization of PBS.

3.5. Triboelectric Properties

3.5.1. Triboelectric Charging of Individual Films

To investigate the triboelectric properties of each individual PBS/MCC film composition, ITO PBS composite films were contact-separated against another ITO electrode (**Figure 4**a). ITO was chosen as contacting material to investigate the individual charging trends of different PBS/MCC composites as material transfer, which governs the charge formation on polymers,[50,51] is not expected from inorganic ITO material.[52] All samples charged negatively after contact with ITO (Figure 4b).

In contact with ITO, pure PBS showed the highest surface charge of −0.078 nC cm^{-2}. All other PBS/MCC samples presented an approximately similar surface charge of ≈−0.020 to −0.040 nC cm^{-2}, with a slight increase in surface charge as MCC content increased from 10% to 70%. The Youngs modulus of ITO glass is significantly higher than PBS (on the order of 190 GPa),[53] thus it is reasonable that the softest polymer (presenting the biggest difference in deformability compared to the ITO) showed the higher surface charge.

Through experimental observations, it has been previously established that when all other chemical and mechanical properties of a polymer bulk remain constant, smoother surfaces exhibit a negative surface charge.[37] Polymer chains subjected to tension possess a lower energy for bond scission. Calculations have shown that the smooth surface can be expected to represent the strained surface, therefore smooth surfaces are under tension during contact separation, and (due to ion adsorption effects) become negatively charged. Similarly, the addition of filler particles increases the stiffness of the film which leads to lower tangential strain upon contact-separation than in pristine PBS polymer.

The trend of surface charge increase from 10% to 70% MCC content occurs as there is increased heterogeneity of the surface of PBS with increasing MCC content, leading to stress concentration that slightly increases the surface charge.

The charge becoming more negative at higher filler concentrations in contact with ITO could be related to individual properties of MCC as it is reported to gain negative contact charge.[54] This triboelectric charging tendency of MCC is in conflict with the tendency of polymer composites to observe positive surface charge when roughness and stiffness is increasing. The observed result aligns well with prior observations,[55] where higher surface charge was measured for softer polymers due to weaker intermolecular bonding and larger effective contact area, in addition to enhanced deformation and friction.[35] However, the critical result here is there is a significant *difference* in surface charge generation between pure PBS and MCC/PBS composites that can be exploited for biodegradable TENG devices.

Further, the charge was measured by contacting different combinations of pristine PBS and the MCC/PBS composite films. The schematic measurement setup is demonstrated in Figure 4c. The charge was measured by contacting with 10 N force and separation by 5 mm with a speed of 10 mm s^{-1} (Table S1, Supporting Information). The charge is shown to be approximately linear with the difference in elastic modulus between the polymer pair. The highest surface charge of 0.03 nC cm^{-2} was measured when pristine PBS is contacted with PBS composite containing 70 wt.% of MCC (**Figure 5**). Notably, contact between pristine PBS and any MCC/PBS composite resulted in a linear trend with elastic modulus difference (Figure S4 and Table S1, Supporting Information), with the variations observed in Figure 4d only occurring between different concentrations of MCC/PBS composites. It is important to note that the other reasons, such as the effect of surface roughening, also cannot be excluded for enhanced charging,[37,41] as the roughness of the films is changing by adding MCC (Figure S2, Supporting Information). However, the roughness change is far from linear and thus cannot be regarded as a dominating effect.

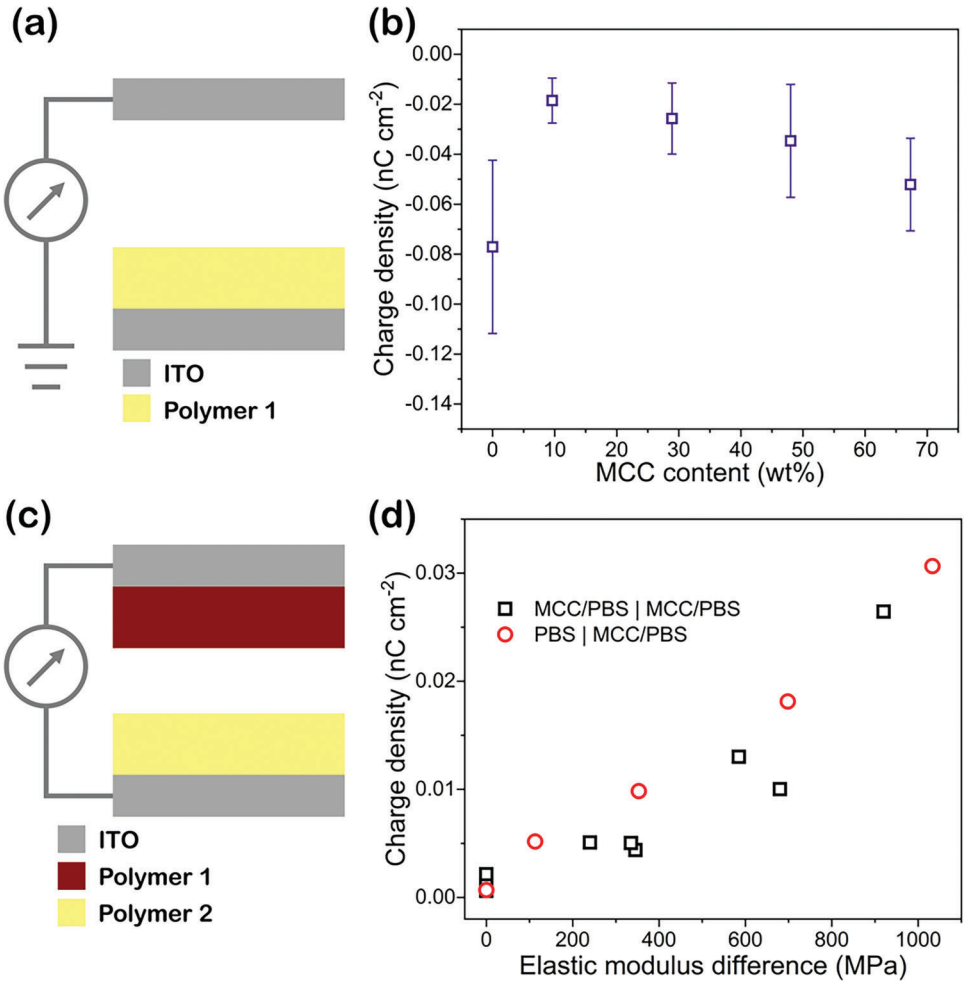

Figure 4. a) Schematic representation of composite films charge measurement; b) charge density of composites with various MCC contents after contact-separation against ITO (error bars represent the standard deviation in charge of 4 samples); c) schematic representation of TENG; d) charge density as a function of the difference in elastic modulus of both contacted nanocomposite films.

For the contact pair of PBS versus PBS/MCC 70% composite, the surface charge density and polarity on each individual film was measured (**Figure 6**). In the experiments, PBS charged negatively -0.012 ± 0.001 nC cm^{-2} while 70 wt.% MCC/PBS composite obtained a positive surface charge $+0.013 \pm 0.001$ nC cm^{-2}. This is in agreement with our previous work where we contacted 196 combinations of different polymers with distinct mechanical properties and demonstrated that soft polymers always observe negative surface charge.[52] Further, the addition of MCC with strong binding to the PBS (as indicated by the rule of mixtures for mechanical properties), will lead to enhanced heterogeneity in surface stress concentration, leading to a propensity for the 70% MCC/PBS composite to charge positively.[37]

The results were confirmed using scanning Kelvin probe measurements (**Figure 7**). For pristine PBS the initial surface potential was measured at 4.75 V and after contact against 70 wt.% MCC/PBS composite it increased by 18% to 5.61 V, while for the 70 wt.% MCC/PBS composite average surface potential increased by 39% – from 1.09 to 1.51 V. The larger relative polarity shift for the MCC/PBS composite will result in a positive surface charge signal being observed in the electrical measurement. The authors note that measured surface potential here is a relative value, and thus it is important to consider the percentage change in value, rather than the total magnitude.

3.5.2. Triboelectric Nanogenerator Performance

Further, we measured the charge density as a function of compression force for a TENG generator device (Figure 4c) constructed using pristine PBS and 70 wt.% MCC/PBS composite (**Figure 8**a).

This force testing showed two linear regimes, with a steep rise in surface charge up to 200 N compression force (reaching ≈0.25 nC cm^{-2}), with a slower increase up to 500 N (reaching 0.35 nC cm^{-2}).

This change to a lower slope at a higher force is likely due to a shift from a purely elastic deformation regime to an elastic/plastic deformation regime. Figure 8b shows the energy density and power density of the same TENG device as a function of load resistance used in voltage measurements using 500 N compression force (Figure S5, Supporting Information). The highest

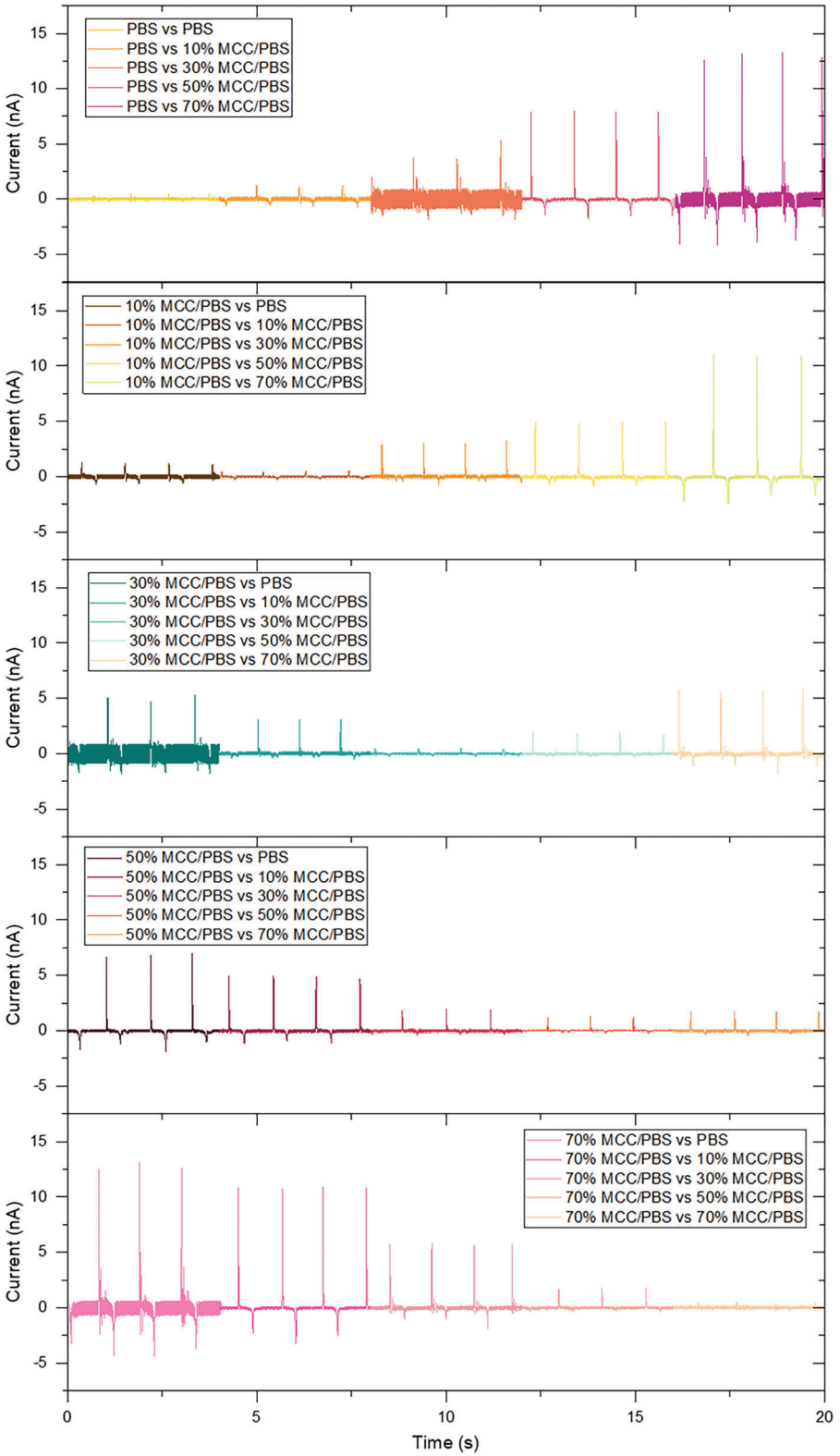

Figure 5. Short-circuit current measurements for contact between MCC/PBS samples with different compositions at 100 mm s^{-1} separation speed.

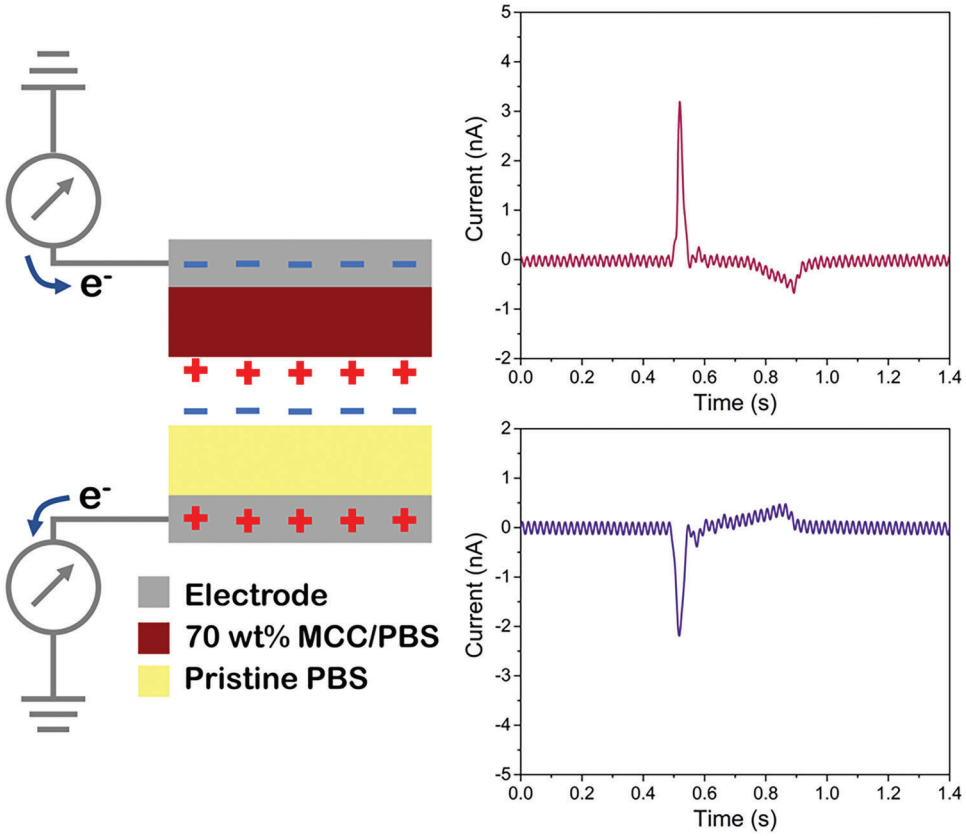

Figure 6. Schematic of the experimental setup for surface charge measurement and the measured current signal from (top) 70 wt.% MCC/PBS in contact with (bottom) pristine PBS.

power density of 1.2 mW m^{-2} was obtained at 550 MΩ load resistance. The PBS | 70% MCC/PBS TENG was used to charge three different capacitors – 22, 47, and 680 nF (Figure 8c,d). During 1 minute of charging (at 500 N force and 1 Hz frequency), 5.1 V was achieved across the 22 nF capacitor with a 286 nJ of energy stored (Figure 8d). For 47 nF capacitor the stored energy was slightly lower – 211 nJ. In the case of 680 nF capacitor stored energy was the lowest – 21 nJ. However, in all cases, the PBS | MCC/PBS TENG is shown to be applicable for mechanical-to-electrical energy transduction.

The charge density calculated from current measurements of PBS | 70% MCC/PBS TENGs using a literature standard 10 N compression force of 0.03 nC cm^{-2} (Figure 8a; and Table S1, Supporting Information) is comparable to the charge of state-of-the-art polymers PDMS | ITO (0.05 nC cm^{-2}) and PTFE | ITO (0.06 nC cm^{-2}), when an identical experimental conditions and testing setup was used.[55]

The electrical output of the TENG device constructed using pristine PBS and 70 wt.% MCC/PBS composite was tested after it had been placed in ambient indoor conditions for 12 weeks to evaluate changes in performance. The TENG device demonstrated no loss in measured current output after this 12-week period. Long-term continuous cycling reveals a small increase in the measured current over 10 000 cycles, demonstrating exceptional stability. The calculated charge density during testing increases from 0.032 to 0.041 nC cm^{-2}. Such an effect is often observed as a majority of polymer materials require some initial contact-separation cycles to achieve a stable saturated signal.[56]

Additionally, we tested the performance at different relative humidity conditions. Results were taken after ≈2500 contact-separation cycles. For example, long-term stability tests were performed at standard RH of 35% (most common conditions) and the calculated charge density was 0.033 nC cm^{-2}. As expected,[57] at low relative humidity (≈25%) the generated current and charge density was higher, it reached 40 nA and 0.111 nC cm^{-2}, respectively (Figure S6, Supporting Information).

3.5.3. Energy and Power Density of TENG

For exploration of surface charge measurements, a moderate translation speed of 100 mm s^{-1} was used (Figure 8), however, to demonstrate the highest possible output from TENG device, we performed triboelectrification tests by applying faster contact-separation of 1000 mm s^{-1}. The results from after contact-separation experiments (**Figure 9**) show 20 μA peak-to-peak short-circuit current measured in the rapid contact-separation (Figure S7, Supporting Information).

The peak observed at separation was used to calculate the surface charge density of 1.36 ± 0.16 nC cm^{-2}. The highest peak-to-peak open-circuit voltage of 420 V was observed at 550 MΩ (Figure S8, Supporting Information). Regarding the

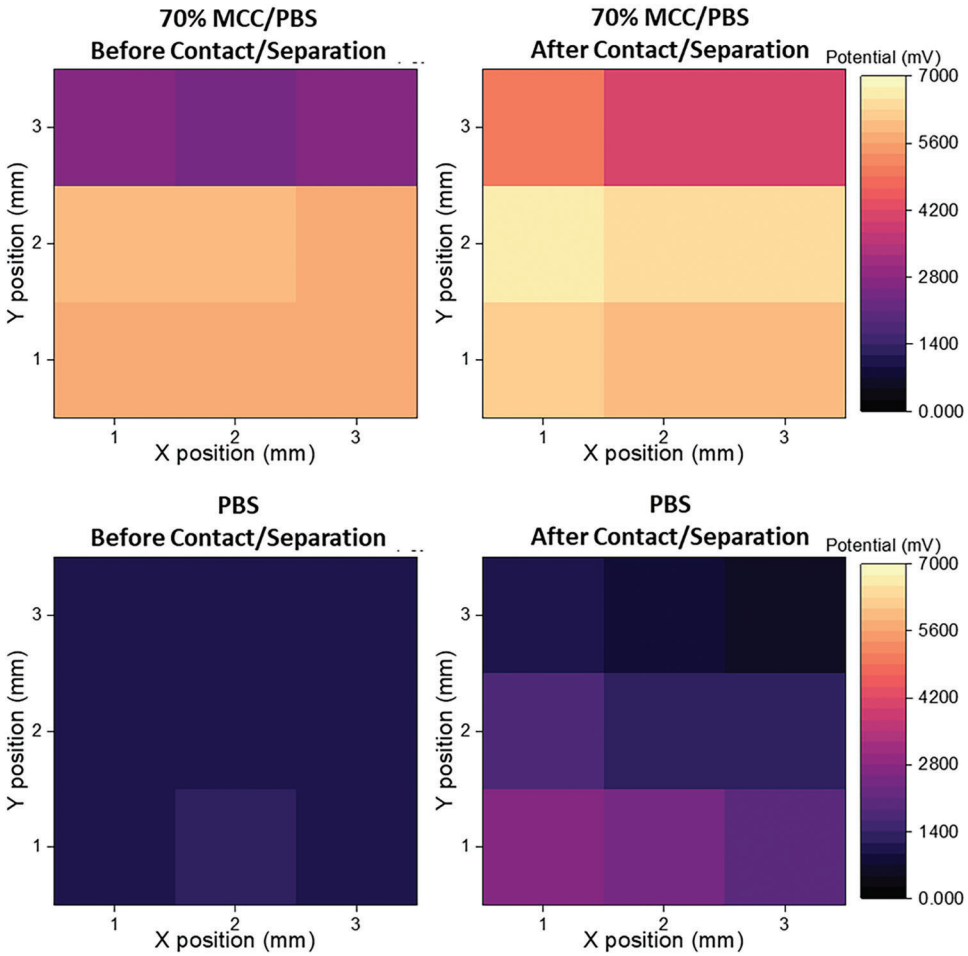

Figure 7. Surface potential maps of PBS and 70 wt.% MCC/PBS composite before and after contact-separation to each other.

power and energy density, the rapid contact-separation tests allowed the biodegradable TENG device to reach a power density of 143 mW m^{-2} at the optimal load resistance of 10 MΩ and an energy density of 2.4 mJ m^{-2} at 550 MΩ (Figure 9). The power density is comparable with values reported for other TENG devices based on biodegradable polymers in contact with synthetic polymers.[23,32] Rapid contact-separation tests reveal that the PBS-PBS/70%MCC TENG device achieves energy and power densities suitable for application in vibration energy harvesting in order to power microdevices.

3.6. Biodegradation Studies in the Composting Conditions

PBS, similarly, to other modern biodegradable plastics and polymers, requires a high molecular weight to obtain excellent mechanical performance properties. Although various types of PBS-degrading microorganisms have been identified,[58] the composition of natural soil is far from optimal for rapidly degrading high molecular weight (50 000 to 200 000) polymers such as PBS.[59] This, in turn, limits the biodegradability of the polymer. Thus, for these materials, industrial composting facilities were introduced as a new waste disposal route.

To achieve composting conditions, the soil needs to be sufficiently wet and the temperature should be above 30 °C. By the method description, 58 °C ensures the high activity of thermophilic bacteria and fungi.[60] It should be noted that it is assumed that biodegradation is mainly a surface process. **Figure 10**a shows visual changes in samples recovered from the compositing soil, while Figure 10b illustrates the mass loss during the biodegradation process. Each photo shows changes between ten-day intervals. It is clear that the higher content of MCC contributes to a faster initial degradation step. The 70 wt.% MCC/PBS composite shows significant discoloration after only 10 days and clear fracturing/disintegration of the film occurs within 30 to 40 days.

At the same time, pristine PBS and composites with 10 and 30 wt.% content of MCC only show slight discoloration after the initial 10 days of composting. The presence of cellulose (MCC) particles inside the composite promotes water absorption into the sample, which results in effects such as swelling. This in turn contributes to increased surface area for biodegradation to occur, especially after the initial polymer layer is broken down by bacteria.[61]

After an initial period of biodegradation, compositions with lower MCC content, crumble between the 40-to-50 days. Visually

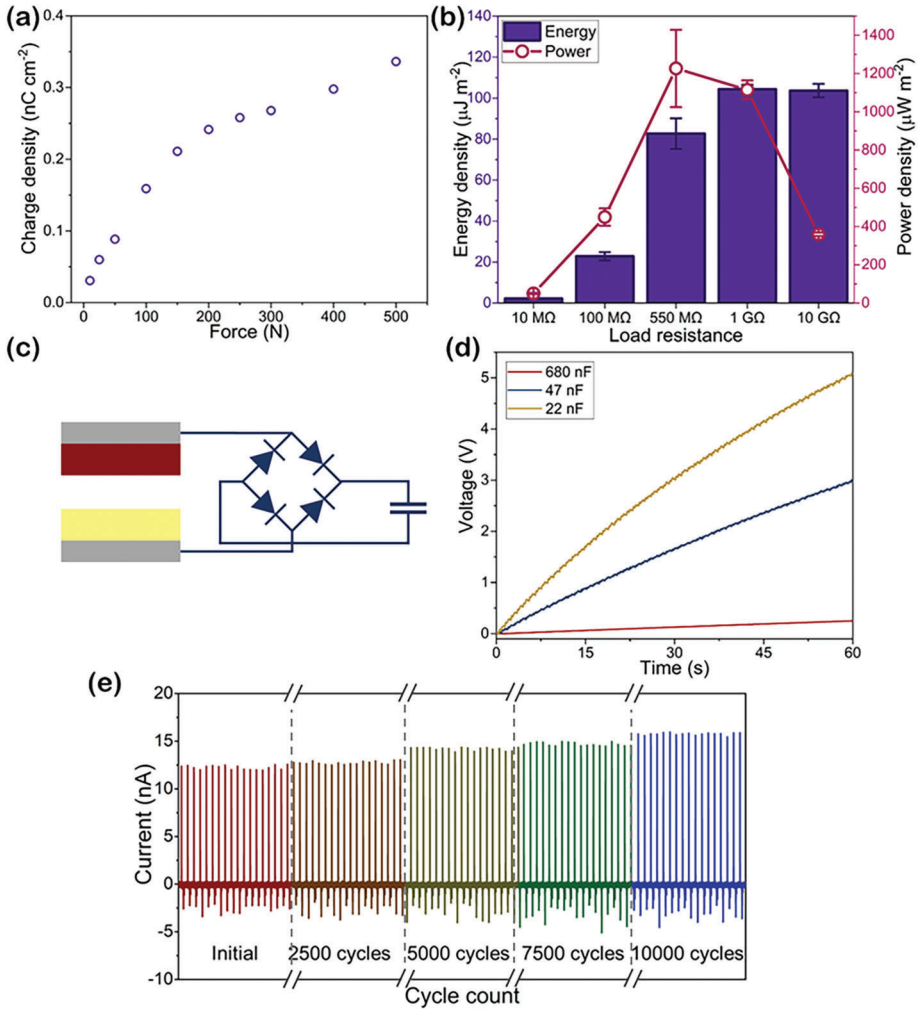

Figure 8. a) Charge density as a function of force for TENG constructed using pristine PBS and PBS composite with 70 wt.% MCC content; b) Energy and power densities at different load resistance values for TENG constructed from pristine PBS and PBS composite with 70 wt.% MCC content; c) Schematic of the circuit including TENG, full bridge rectifier and capacitor; d) Voltage across various capacitors during 60 s charging from the TENG constructed using pristine PBS and PBS composite with 70 wt.% MCC content; e) Short-circuit current of PBS-PBS/70%MCC TENG tested for 10 000 contact-separation cycles (only a small number of cycles immediately after the stated cycle number are shown).

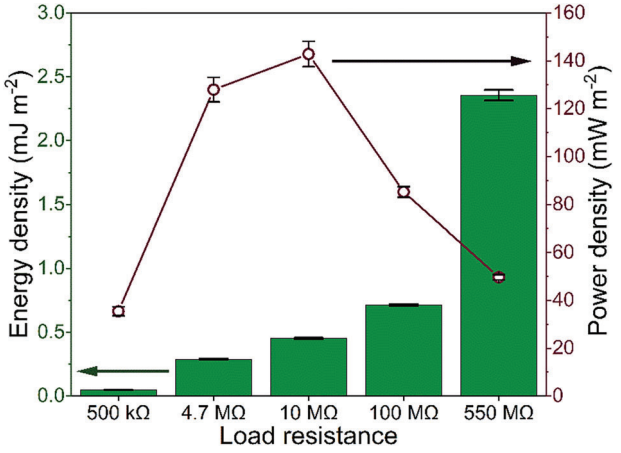

Figure 9. Energy density and power density as a function of load resistance for PBS-PBS/70%MCC TENG tested in the high-speed contact-separation.

and also by mass, it can be seen that cellulose content cannot significantly reduce the final degradation time. The difference in remaining mass between composites with 10 and 70 wt.% of MCC never exceeds 20%, while their MCC content difference by weight is 60%. This stems from the limitation of the surface biodegradation process and limited contact with the bacteria.

Kunioka et al. studied PBS and cellulose biodegradation in composting conditions at 58 °C and measured evolved CO_2 (ISO 14855-2).[62] The authors reported that microcrystalline cellulose with a particle size of less than 20 μm biodegraded fully between 40 and 50 days, while PBS achieved ≈80% mass loss in 74 days. Buenaventurada et al. similarly studied PBS biodegradation in accordance with ISO 14855-2.[63] In this case, the authors reported ≈60% mass loss for PBS after 70 days and ≈95% mass loss for PBS blended with 40 wt.% of cotton fibers. These reports align well with the test results achieved in this work, where PBS lost 80.6% of the mass in 70 days and composites lost from 84.8 to 92.7% of their initial mass depending on cellulose content.

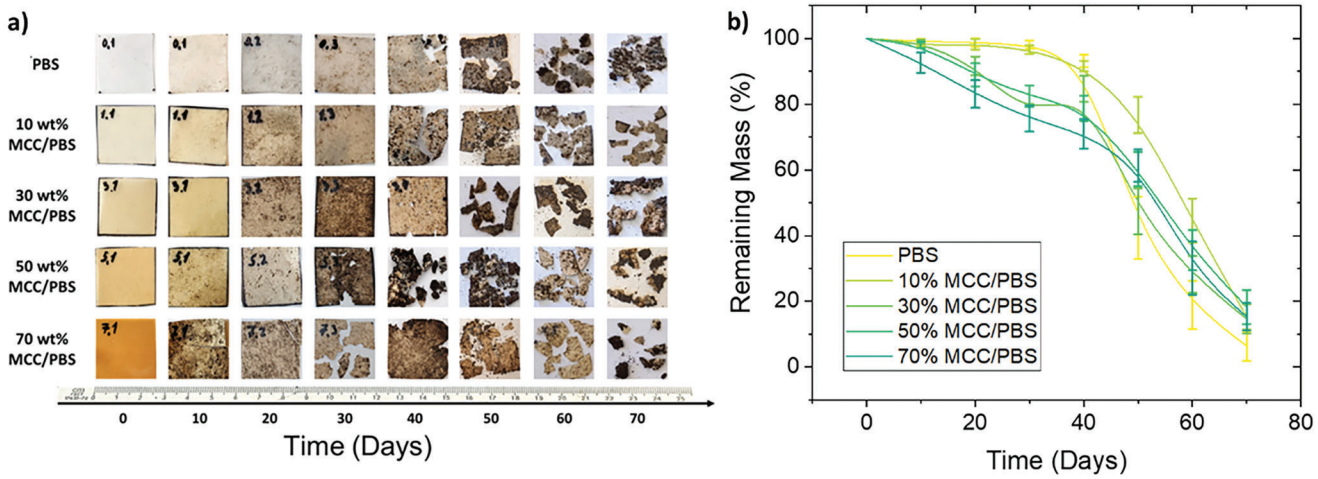

Figure 10. a) Visual changes of PBS and PBS/MCC composites during the biodegradation process in the composting conditions; b) Mass loss of PBS and PBS/MCC composites during biodegradation in the composting condition.

The reliance on thermally activated degradation of the PBS composites is a critical advantage of these TENG devices. During conventional operation, there is no degradation to the material, as shown by the continued high performance over 10000 cycles (Figure 7e). However, if the TENG is disposed of in a landfill the high heat conditions will initatiate the degradation process enabling mitigation of environmental consequences from TENG disposal.

There are an array of other pathways that can be studied to degrade polymers, particularly for cellulose-based materials.[24–28,64] Critically for TENGs, the long cycle life (in this case 10 000 cycles) requires thermal and chemical stability of the polmyers in air. Thus to control the timeline of degradation (i.e., post-use disposal), the use of compositing or other systems[64] that directly initiate degradation provide a promising pathway to a circular economy of TENGs.

3.7. Benchmarking Biodegradable TENGs

While many biodegradable polymers have been tested in contact with synthetic polymers[23,32] or metals,[65] there are fewer reports of biopolymer-biopolymer based contact pairs. **Table 3** summarises the exemplar material combinations from the literature from such biopolymer-biopolymer contact pairs.[66–69] Pan et al.[66] and Edberg et al.[67] describe the use of fibers or nanofibers of polymers to achieve a power density >1 W m^{-2}. The power density of 140 mW m^{-2} described herein is obtained for films with relatively homogenous surface roughness, and is comparable to the best reported biopolymer-biopolymer film based TENGs in literature.[68,69] The distinction between film and fiber based TENGs is critical as the stress concentration achieved at sharp aspect ratio features creates significant bond scission and enhances charge transfer.[37,70] These factors, in addition to greater compressibilty for fibrous films, and leads to significantly higher power densities for all fiber TENGs.[71,72]

4. Conclusion

In conclusion, we have demonstrated how to achieve and control triboelectrification in PBS polymer and MCC/PBS composites. These MCC/PBS composites are biodegradable via compositing at mildly elevated temperatures. This provides a tool to have highly stable TENGs operate for 1000s of cycles, followed by degradation after disposal. The proposed approach can be potentially extended to other biodegradable polymers. The considerable triboelectric surface charge can be measured by contacting two PBS films with different MCC content, correlated to their individual mechanical properties. The PBS materials are applicable for preparing TENG devices from single triboelectric material capable to generate power density of 143 mW m^{-2} and charge density of 1.36 nC cm^{-2}. The triboelectric PBS films are biodegradable and lose 80.6% to 92.7% of weight in compost depending on cellulose content, providing a solution for microplastic and polymer pollution caused by discarded TENGs. The development of high performance TENGs that are able to be compostable, moves away from the paradigm of single use TENGs, providing a route

Table 3. Comparison of Biopolmyer-Biopolmyer TENG devices.

Material 1	Material 2	Power density [W m^{-2}]	Ref.
Nanostructured Gelatin Film	Electrospun Polylactic Acid Membrane	1.25	Pan et al.[66]
Lignin Fiber	Nitrocellulose Fiber Mat	1.60	Edberg et al.[67]
Chitosan Film	Poly-L-lactic Acid Aligned Electrospun Fibers	0.065	Khandelwal et al.[68]
Porous poly-ϵ-caprolactone/ethyl cellulose film	Poly-ϵ-caprolactone Electrospun Fibers	0.16	Fan et al.[69]
Compression Moulded PBS Film	Compression Moulded 70% MCC/PBS Film	0.14	This work

to address both Affordable and Clean Energy and Responsible Consumption and Production United Nations Sustainable Development Goals.

Supporting Information

Supporting Information is available from the Wiley Online Library or from the author.

Acknowledgements

This work was supported by Latvian Council of Science in the framework of FLPP "Printed biopolymer 4D TENG device for mechanical energy harvesting" (lzp-2022/1-0485). Roughness measurements were performed on equipment located at the Center of Excellence at the Institute of Solid State Physics, University of Latvia, which was supported by European Union's Horizon 2020 Framework Programme H2020-WIDESPREAD-01-2016-2017-TeamingPhase2 under Grant Agreement No. 739508, project CAMART2. P.C.S. acknowledges support from RMIT University through the RMIT Vice-Chancellor's Research Fellowship Scheme.

Open access publishing facilitated by RMIT University, as part of the Wiley - RMIT University agreement via the Council of Australian University Librarians.

Conflict of Interest

The authors declare no conflict of interest.

Data Availability Statement

The data that support the findings of this study are available from the corresponding author upon reasonable request.

Keywords

biodegradability, celluloses, composites, polybutylene succinate, triboelectric nanogenerators

Received: June 27, 2023
Revised: August 15, 2023
Published online: August 21, 2023

[1] Z. L. Wang, *Adv. Energy Mater.* **2020**, *10*, 2000137.
[2] Y. Zou, P. Tan, B. Shi, H. Ouyang, D. Jiang, Z. Liu, H. Li, C. Wang, X. Qu, L. Zhao, Y. Fan, Z. L. Wang, Z. Li, *Nat. Commun.* **2019**, *10*, 2695.
[3] G. Zhu, W. Q. Yang, T. Zhang, Q. Jing, J. Chen, Y. S. Zhou, P. Bai, Z. L. Wang, *Nano Lett.* **2014**, *14*, 3208.
[4] T. Jin, Z. Sun, L. Li, Q. Zhang, M. Zhu, Z. Zhang, G. Yuan, T. Chen, Y. Tian, X. Hou, C. Lee, *Nat. Commun.* **2020**, *11*, 5381.
[5] W. Li, Y. Pei, C. Zhang, A. G. P. Kottapalli, *Nano Energy* **2021**, *84*, 105865.
[6] S. Li, J. Jiang, N. Zhai, J. Liu, K. Feng, Y. Chen, Z. Wen, X. Sun, J. Zhong, *Nano Energy* **2022**, *93*, 106870.
[7] B. Zhang, C. Zhang, O. Yang, W. yuan, Y. Liu, L. He, Y. Hu, Z. Zhao, L. Zhou, J. Wang, Z. L. Wang, *ACS Nano* **2022**, *16*, 15286.
[8] X. Liu, T. Chen, F. Qian, Z. Guo, F. X. Lin, X. Wang, K. Chen, in *Proc. of the 15th Annual Int. Conf. on Mobile Systems, Applications, and Services*, Association for Computing Machinery, New York, NY, USA **2017**, p. 385.
[9] M. Kim, D. Park, M. M. Alam, S. Lee, P. Park, J. Nah, *ACS Nano* **2019**, *13*, 4640.
[10] J. Li, N. A. Shepelin, P. C. Sherrell, A. V. Ellis, *Chem. Mater.* **2021**, *33*, 4304.
[11] M. Wang, N. Zhang, Y. Tang, H. Zhang, C. Ning, L. Tian, W. Li, J. Zhang, Y. Mao, E. Liang, *J. Mater. Chem. A* **2017**, *5*, 12252.
[12] A. Šutka, K. Mālnieks, A. Linarts, M. Timusk, V. Jurķāns, I. Gorņevs, J. Blūms, A. Bērziņa, U. Joost, M. Knite, *Energy Environ. Sci.* **2018**, *11*, 1437.
[13] S. Pan, Z. Zhang, *Friction* **2019**, *7*, 2.
[14] D. J. Lacks, T. Shinbrot, *Nat. Rev. Chem.* **2019**, *3*, 465.
[15] H. Baytekin, B. Baytekin, J. Incorvati, B. Grzybowski, *Angew. Chem., Int. Ed.* **2012**, *51*, 4843.
[16] Z. L. Wang, A. C. Wang, *Mater. Today* **2019**, *30*, 34.
[17] J. Chen, J. Wu, P. C. Sherrell, J. Chen, H. Wang, W.-X. Zhang, J. Yang, *Adv. Sci.* **2022**, *9*, 2103764.
[18] B.-G. Park, C. Lee, Y.-J. Kim, J. Park, H. Kim, Y. Jung, J. S. Ko, S-W. K., J.-H. Lee, H. Cho, *Nano Energy* **2022**, *100*, 107433.
[19] R. Pan, W. Xuan, J. Chen, S. Dong, H. Jin, X. Wang, H. Li, J. Luo, *Nano Energy* **2018**, *45*, 193.
[20] L. Valentini, M. Cardinali, J. Kenny, *J. Polym. Sci., Part B: Polym. Phys.* **2014**, *52*, 859.
[21] C. Ma, S. Gao, X. Gao, M. Wu, R. Wang, Y. Wang, Z. Tang, F. Fan, W. Wu, H. Wan, W. Wu, *InfoMat* **2019**, *1*, 116.
[22] Z. Niu, W. Cheng, M. Cao, D. Wang, Q. Wang, J. Han, Y. Long, G. Han, *Nano Energy* **2021**, *87*, 106175.
[23] S. Hao, J. Jiao, Y. Chen, Z. L. Wang, X. Cao, *Nano Energy* **2020**, *75*, 104957.
[24] Y. Shao, C.-P. Feng, B.-W. Deng, B. Yin, M.-B. Yang, *Nano Energy* **2019**, *62*, 620.
[25] H. Yu, Y. Shao, C. Luo, Y. Li, H.-Z. Ma, H.-Y. Zhang, B. Yin, J.-B. Shen, M.-B. Yang, *Composites, Part A* **2021**, *151*, 106646.
[26] C. Luo, Y. Shao, H. Yu, H. Ma, Y. Zhang, B. Yin, M.-B. Yang, *ACS Sustainable Chem. Eng.* **2022**, *10*, 13050.
[27] C. Luo, H. Ma, H. Yu, Y. Zhang, Y. Shao, B. Yin, K. Ke, L. Zhou, K. Zhang, M.-B. Yang, *ACS Sustainable Chem. Eng.* **2023**, *11*, 9424.
[28] Q. Niu, H. Wei, B.-S. Hsiao, Y. Zhang, *Nano Energy* **2022**, *96*, 107101.
[29] H. Kim, S. Choi, Y. Hong, J. Chung, J. Choi, W.-K. Choi, I. W. Park, S. H. Park, H. Park, W.-J. Chung, K. Heo, M. Lee, *Appl. Mater. Today* **2021**, *22*, 100920.
[30] G. Khandelwa, N. P. M. Joseph Raj, N. R. Alluri, S.-J. Kim, *ACS Sustainable Chem. Eng.* **2021**, *9*, 9011.
[31] J. Bang, I. K. Moon, Y. P. Jeon, B. Ki, J. Oh, *Appl. Surf. Sci.* **2021**, *567*, 150806.
[32] C. Zhang, X. Lin, N. Zhang, Y. Lu, Z. Wu, G. Liu, S. Nie, *Nano Energy* **2019**, *6*, 104126.
[33] Y. Mi, Y. Lu, Y. Shi, Z. Zhao, X. Wang, J. Meng, X. Cao, N. Wang, *Polymers* **2023**, *15*, 222.
[34] S. Chao, H. Ouyang, D. Jiang, Y. Fan, Z. Li, *EcoMat* **2021**, *3*, 12072.
[35] L. Lapčinskis, A. Linarts, K. Mālnieks, H. Kim, K. Rubenis, K. Pudzs, K. Smits, A. Kovaļovs, K. Kalniņš, A. Tamm, C. K. Jeong, A. Šutka, *J. Mater. Chem. A* **2021**, *9*, 8984.
[36] A. Šutka, L. Lapčinskis, O. Verners, L. Ģērmane, K. Smits, A. Pludons, S. Gaidukovs, I. Jerāne, M. Zubkins, K. Pudzs, P. C. Sherrell, J. Blums, *Adv. Mater. Technol.* **2022**, *7*, 2200162.
[37] O. Verners, L. Lapčinskis, L. Ģērmane, A. Kasikov, M. Timusk, K. Pudzs, A. V. Ellis, P. C. Sherrell, A. Šutka, *Nano Energy* **2022**, *104*, 107914.
[38] O. Platnieks, S. Gaidukovs, A. Barkane, G. Gaidukova, L. Grase, V. K. Thakur, I. Filipova, V. Fridrihsone, M. Skute, M. Laka, *Molecules* **2020**, *25*, 121.
[39] S. Briede, M. Jurinovs, S. Nechausov, O. Platnieks, S. Gaidukovs, *Mol. Syst. Des. Eng.* **2022**, *7*, 1434.

[40] O. Platnieks, S. Gaidukovs, N. Neibolts, A. Barkane, G. Gaidukova, V. K. Thakur, *Mater. Today Chem.* **2020**, *18*, 100351.
[41] A. Šutka, K. Mālnieks, L. Lapčinskis, M. Timusk, K. Kalniņš, A. Kovaļovs, J. Bitenieks, M. Knite, D. Stevens, J. Grunlan, *Phys. Chem. Chem. Phys.* **2020**, *22*, 13299.
[42] L. Ģērmane, L. Lapčinskis, M. Iesalnieks, A. Šutka, *Mater. Adv.* **2023**, *4*, 875.
[43] J. Ostrowska, W. Sadurski, M. Paluch, P. Tynski, J. Bogusz, *Polym. Int.* **2019**, *68*, 1271.
[44] O. Platnieks, A. Sereda, S. Gaidukovs, V. K. Thakur, A. Barkane, G. Gaidukova, I. Filipova, A. Ogurcovs, V. Fridrihsone, *Ind. Crops Prod.* **2021**, *169*, 113669.
[45] B. Govedarica, M. Škarabot, I. Ilić, O. Planinšek, I. Muševič, S. Srčič, *Procedia Eng.* **2011**, *10*, 2857.
[46] H. S. Kim, *Mater. Sci. Eng. A* **2000**, *289*, 30.
[47] X. Li, B. Lei, Z. Lin, L. Huang, S. Tan, X. Cai, *Mater. Des.* **2014**, *53*, 419.
[48] M. Yasuniwa, T. Satou, *J. Polym. Sci., Part B: Polym. Phys.* **2002**, *40*, 2411.
[49] D. G. Papageorgiou, E. Zhuravlev, G. Z. Papageorgiou, D. Bikiaris, K. Chrissafis, C. Schick, *Polymer* **2014**, *55*, 6725.
[50] H. T. Baytekin, A. Z. Patashinski, M. Branicki, B. Baytekin, S. Soh, B. A. Grzybowski, *Science* **2011**, *333*, 308.
[51] T. Mazur, B. A. Grzybowski, *Chem. Sci.* **2017**, *8*, 2025.
[52] P. C. Sherrell, A. Šutka A, N. A. Shepelin, L. Lapcinskis, O. Verners, L. Germane, M. Timusk, R. A. Fenati, K. Malnieks, A. V. Ellis, *ACS Appl. Mater. Interfaces* **2021**, *13*, 44935.
[53] B. K. Lee, Y. H. Song, J. B. Yoon, *2009 IEEE 22nd Int. Conf. on Micro Electro Mechanical Systems*, Sorrento, Italy, January **2009**.
[54] Y. Li, N. Wang, S. Wang, B. Li, E. Ye, X. Loh, Z. Li, *Sustainable Energy Fuels* **2023**, *7*, 2087.
[55] A. Šutka, K. Mālnieks, L. Lapčinskis, P. Kaufelde, A. Linars, A. Berzina, R. Zabels, V. Jurkans, I. Gornevs, J. Blums, M. Knite, *Energy Environ. Sci.* **2019**, *12*, 2417.
[56] F. Chowdhury, A. Sowinski, M. Ray, A. Passalacqua, P. Mehrani, *J. Electrost.* **2018**, *91*, 9.
[57] Y. I. Sobolev, W. Adamkiewicz, M. Siek, B. A. Grzybowski, *Nat. Phys.* **2022**, *18*, 1347.
[58] H. Mao, H. Liu, Z. Gao, T. Su, Z. Wang, *Polym. Degrad. Stab.* **2015**, *114*, 1.
[59] H.-S. Kim, H.-J. Kim, W.-J. Lee, I.-G. Choi, *Polym. Degrad. Stab.* **2006**, *91*, 1117.
[60] R. Mouhoubi, M. Lasschuijt, S. R. Carrasco, H. Gojzewski, F. R. Wurm, *Waste Manage.* **2022**, *154*, 36.
[61] S. Gaidukovs, O. Platnieks, G. Gaidukova, O. Starkova, A. Barkane, S. Beluns, V. K. Thankur, *J. Polym. Environ.* **2022**, *30*, 1435.
[62] M. Kunioka, F. Ninomiya, M. Funabashi, *Int. J. Mol. Sci.* **2009**, *10*, 4267.
[63] B. P. Calabia, F. Ninomiya, H. Yagi, A. Oishi, K. Taguchi, M. Kunioka, M. Funabashi, *Polymers* **2013**, *5*, 128.
[64] J. Zhou, H. Wang, C. Du, D. Zhang, H. Lin, Y. Chen, J. Xiong, *Adv. Energy Sustainable Res.* **2021**, *3*, 2100161.
[65] P. K. Sarkar, T. Kamilya, S. Acharya, *ACS Appl. Energy Mater.* **2019**, *2*, 5507.
[66] R. Pan, W. Xuan, J. Chen, S. Dong, H. Jin, X. Wang, H. Li, J. Luo, *Nano Energy* **2018**, *45*, 193.
[67] J. Edberg, M. Y. Mulla, O. Hosseinaei, N. H. Alvi, V. Beni, *Global Challenges* **2022**, *6*, 2200058.
[68] G. Khandelway, G. Min, X. Karagiorgis, R. Dahiya, *Nano Energy* **2023**, *110*, 108325.
[69] C. Fan, J. Huang, A. Mensah, Z. Long, J. Sun, Q. Wei, *Cell Rep. Phys. Sci.* **2022**, *3*, 101012.
[70] A. Sutka, L. Lapcinskis, D. He, H. Kim, J. D. Berry, J. Bai, M. Knite, A. V. Ellis, C. K. Jeong, P. C. Sherrell, *Adv. Mater. Interfaces* **2023**, 2300323.
[71] A. Linarts, P. C. Sherrell, K. Malnieks, A. V. Ellis, A. Sutka, *Small* **2023**, *19*, 202205563.
[72] W. Paosangthong, R. Torah, S. Beeby, *Nano Energy* **2019**, *55*, 401.